Coordinated Bidirectional Power Flow Management with Power Quality Improvement in AC-DC Hybrid Micro-grid under Unbalanced Scenario

Nagaraj C[1*], K Manjunatha Sharma[2]
1- Department of Electrical and Electronics Engineering, National Institute of Technology Karnataka, Surathkal, India.
Email: assiniraj@gmail.com (Corresponding author)
2- Department of Electrical and Electronics Engineering, National Institute of Technology Karnataka, Surathkal, India.
Email: manjunatha.sharma@gmail.com

Received: July 2018 Revised: October 2018 Accepted: November 2018

ABSTRACT:
Nowadays electrical power system is highly complex due to the increase in load demand and distributed generations. Further, the intermittent renewable sources and non-linear power electronic loads connected to the grid deteriorates the power quality of the system. Also, a large number of DC loads like LED lights are connected to the AC distribution system to save energy consumption. These issues can be effectively addressed using the smart micro-grid system. In an individual AC or DC micro-grid, the higher number of AC-DC-AC/DC-AC-DC power conversion stages lead to an increased power loss. Therefore, in this paper, an AC-DC hybrid micro-grid topology is proposed, wherein, AC sources and AC loads are connected to AC grid while DC sources and DC loads are connected to DC grid, consequently, the power conversion losses reduce. The shunt active power filter based 3-phase 4-leg bidirectional interlinking converter using d-q reference current method with PI control is proposed to accomplish the inverter-based and rectifier-based power exchange between AC and DC sub-grids with harmonic current compensation under various grid and load conditions. The analysis is carried out in MATLAB/SIMULINK and results proving the improved power quality.

KEYWORDS: Bidirectional Interlinking Converter, Common Connecting Point, Hybrid Micro-Grid, Hysteresis Comparator Control, Shunt Active Power Filter.

1. INTRODUCTION

Due to the greater number of DC loads and renewable sources connecting to the mains, the present AC distribution system has transformed to a smart micro-grid system. Micro-grid could be classified into AC and DC types, which facilitate the flexible injection of powers from various renewable energy sources and loads to the mains. Micro-grid suffers from power generation problems because of the intermittent renewable sources and power electronics applications. Furthermore, the significant amount of non-linear loads in the system deteriorates power quality. To overcome this issue, a Sunt Ative Power Filter (SAPF) is used to limit the grid current harmonics with simultaneous real and VAR power control [1].

Most of the papers published on micro-grids are limited to converter control of individual AC or DC micro-grid, studying the power flow control, voltage and frequency control, etc. In an AC micro-grid [2-5], DC renewable sources are converted to AC through DC-DC boosters and DC-AC inverters in order to connect with AC grid. Also, AC-DC and DC-DC converters are necessary to supply distinct DC voltages for DC loads including LED lights, as shown in Fig. 1(a). In DC micro-grid [6-10], AC renewable sources are converted to DC in order to connect DC grid and DC-AC inverters are necessary to supply AC loads, as shown in Fig. 1(b).

In [2-10], DC-AC-DC/AC-DC-AC power conversion losses are high. An AC/DC hybrid micro-grid (HM) in which AC sources and AC loads are connected to AC grid as well as DC sources and DC loads are connected to DC grid in order to reduce the multiple power conversion losses, as shown in Fig. 1(c) [11-14]. The AC-DC HM structure [15-17] is the most promising one in the near future, which requires more coordination for voltage and power control due to various sources connected to both AC and DC bus links through the bidirectional interlinking converter (BIC). However, the power control management of AC-DC HM is more complicated compared to an

individual AC or DC micro-grid.

The application of SAPF in micro-grid is extensively studied only with coupled renewable energy sources, as applied to unidirectional power flow transfer. Thus, the control techniques are concentrated on proper power transfer to the AC grid side with active power filtering in both AC coupled renewable sources [18-21] and DC coupled renewable sources [22-28]. Thus, in [11-14], the role of BIC is studied for bidirectional power exchange between AC and DC grids alone without concentrating on the power quality improvement.

With this motivation, bidirectional power flow applications with harmonic current mitigation for the AC-DC HM structure consisting of PV array and DC load at DC bus link and DFIG based variable speed WECS and AC linear and non-linear loads at AC bus link connected to the mains are proposed in this paper. The main motive of this strategy is to supply quality power generated from the grid interlinking hybrid PV and DFIG wind energy sources with the minimum power conversions. The SAPF based 3-phase 4-leg BIC using d-q reference current method with PI control accomplishes the inverter-based and rectifier-based power exchange between AC and DC sub-grids with harmonic current compensation simultaneously at the common connecting point (CCP) under various grid and load conditions. The analysis is carried out using MATLAB/SIMULINK and the obtained results have validated the improved power quality. This paper is described as follows. Section 2 presents the overall system description. In section 3 the control methods for BIC is demonstrated. The simulation results for different case studies are explained in section 4. Section 5 presents the conclusions and future scope.

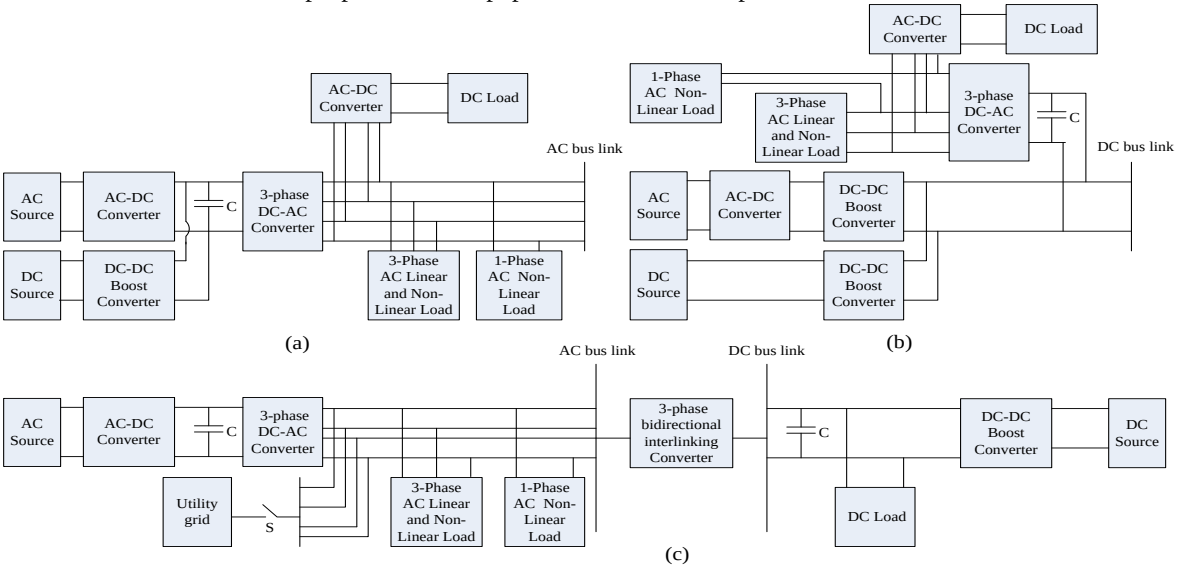

Fig. 1. Block diagram of (a) AC HM system, (b) DC HM system and (c) Proposed AC-DC HM system.

2. OVERALL SYSTEM DESCRIPTION

The power conversion losses are minimum with proposed AC-DC HM system (Fig. 1(C)) over individual AC HM system (Fig. 1(a)) or DC HM system (Fig. 1(b)). The block diagram of the proposed system comprises of DC power source and DC load connected to DC bus interlinking with AC power source and AC linear and non-linear loads connected to AC bus through BIC. The various subsystems of the proposed system are modelled as follows,

2.1. Modeling of PV Array

The I-V characteristic equation of a PV array is given below and its simulation parameters are tabulated in Table 1.

Table 1. Parameters for PV array model [29,30].

Parameters	Values
Short circuit current	I_{SC}=3.87A
Open circuit voltage	V_{OC}=42.1V
No. of series cells	N_S=72
No. of series string modules	N_{SS}=20
No. of parallel string modules	N_{PP}=20
Ideality factor	a=1.3997
Boltzmann constant	K=1.38E^{-23}J/K
Electron charge	Q=1.602E^{-19}C
Current temperature coefficient	K_I=3.2E^{-3}A/K
Voltage temperature coefficient	K_V=-0.1230V/K
Reference temperature	T_{REF}=298.15K
Nominal temperature	T=298.15K

$$I_m = I_{pv}N_{pp} - I_o N_{pp}\left[\exp\left(\frac{V + R_s\left(\frac{N_{ss}}{N_{pp}}\right)I}{V_t a N_{ss}}\right) - 1\right] \quad (1)$$

Where I_{pv} – photo current which varies continuously depends on the intermittent irradiation level and temperature as follows,

$$I_{pv} = \left(I_{pv,n} + K_i \Delta T\right)\frac{G}{G_n} \quad (2)$$

V_t is the thermal voltage given by,

$$V_t = \frac{KTN_s}{q} \quad (3)$$

$I_{pv,n}$ is the photo current generated at actual condition expressed as,

$$I_{pv,n} = \left(R_p + R_s\right)\frac{I_{sc,n}}{R_p} \quad (4)$$

ΔT is the change in actual and reference temperature as follows,

$$\Delta T = \left(T - T_{ref}\right) \quad (5)$$

I_0 is the temperature dependent diode saturation current given as follows,

$$I_0 = \frac{I_{sc,n} + K_i \Delta T}{\exp\left(\frac{V_{oc,n} + K_v \Delta T}{aV_t}\right) - 1} \quad (6)$$

2.2. Modeling of DFIG Variable Wind Speed

If the power output P_m from a DFIG wind depends on its speed and is given by,

$$P_m = 0.5\rho V_w^3 A C_p(\lambda, \beta) \quad (7)$$

The modelling equations for DFIG are required for its control. The voltage equations of an induction motor in a d-q rotating frame are

$$\begin{bmatrix} u_{ds} \\ u_{qs} \\ u_{dr} \\ u_{qr} \end{bmatrix} = \begin{bmatrix} -R_s & 0 & 0 & 0 \\ 0 & -R_s & 0 & 0 \\ 0 & 0 & R_r & 0 \\ 0 & 0 & 0 & R_r \end{bmatrix} \begin{bmatrix} i_{ds} \\ i_{qs} \\ i_{dr} \\ i_{qr} \end{bmatrix} + P \begin{bmatrix} \lambda_{ds} \\ \lambda_{qs} \\ \lambda_{dr} \\ \lambda_{qr} \end{bmatrix} + \begin{bmatrix} -\omega_1\lambda_{qs} \\ \omega_1\lambda_{ds} \\ -\omega_2\lambda_{qr} \\ \omega_2\lambda_{dr} \end{bmatrix} \quad (8)$$

Where

$$\begin{bmatrix} \lambda_{ds} \\ \lambda_{qs} \\ \lambda_{dr} \\ \lambda_{qr} \end{bmatrix} = \begin{bmatrix} -L_s & 0 & 0 & 0 \\ 0 & -L_s & 0 & 0 \\ 0 & 0 & L_r & 0 \\ 0 & 0 & 0 & L_r \end{bmatrix} \begin{bmatrix} i_{ds} \\ i_{qs} \\ i_{dr} \\ i_{qr} \end{bmatrix} \quad (9)$$

The DFIG dynamic equations are as follows,

$$\frac{J}{n_p}\frac{d\omega_r}{dt} = T_m - T_{em} \quad (10)$$

$$T_{em} = n_p L_m\left(i_{qs}i_{dr} - i_{ds}i_{qr}\right) \quad (11)$$

$$\omega_2 = \omega_1 - \omega_r \quad (12)$$

$$\lambda_{ds} = 0, \lambda_{qs} = 0 \quad (13)$$

Substituting (12) and (13) in (8) to obtain the equations in the stator voltage oriented reference frame are given below and the simulation parameters for DFIG wind model are tabulated in Table 2.

$$T_{em} = n_p\left(L_m / L_s\right)\lambda_s i_{dr} \quad (14)$$

$$u_{dr} = R_r i_{dr} + \sigma L_r \frac{di_{dr}}{dt} - \left(\omega_1 - \omega_r\right)\left(L_m i_{qs} + L_r i_{qr}\right) \quad (15)$$

Table 2. Parameters for DFIG wind model [12].

Parameters	Values
Actual power	P_{nom}=50kW
Actual Voltage	V_{nom}=400V
Stator resistance	R_s=0.00706pu
Stator inductance	L_s=0.171pu
Rotor resistance	R_r=0.005pu
Rotor inductance	L_r=0.156pu
Mutual inductance	L_m=0.156pu
Rotor inertia constant	J=3.1s
No. of poles	n_p=6
Actual DC link voltage of back to back converter	V_{dc_nom}=800V
Actual mechanical power	P_m=45kW

$$u_{qr} = R_r i_{qr} + \sigma L_r \frac{di_{qr}}{dt} + \left(\omega_1 - \omega_r\right)\left(L_m i_{ds} + L_r i_{qr}\right) \quad (16)$$

Where

$$i_{ds} = -\frac{L_m}{L_s} i_{dr} \quad (17)$$

$$\sigma = -\frac{L_s L_r - L_m^2}{L_s L_r} \quad (18)$$

3. CONTROL METHODS FOR AC-DC HM

The proposed controller plays a key role in the coordination of the converters and the mains which supplies a continuous, highly efficient and quality power to variable DC and AC linear and non-linear loads under intermittent solar-wind green energy sources with balanced and unbalanced grid conditions. The overall control diagram of the proposed AC-DC HM is depicted in Fig. 2 and discussed in this section.

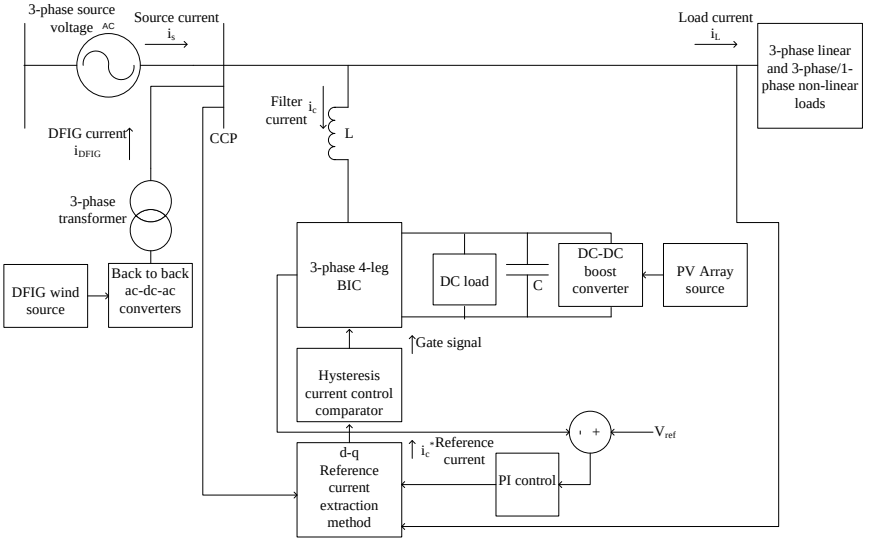

Fig. 2. Overall control diagram of the proposed AC-DC HM.

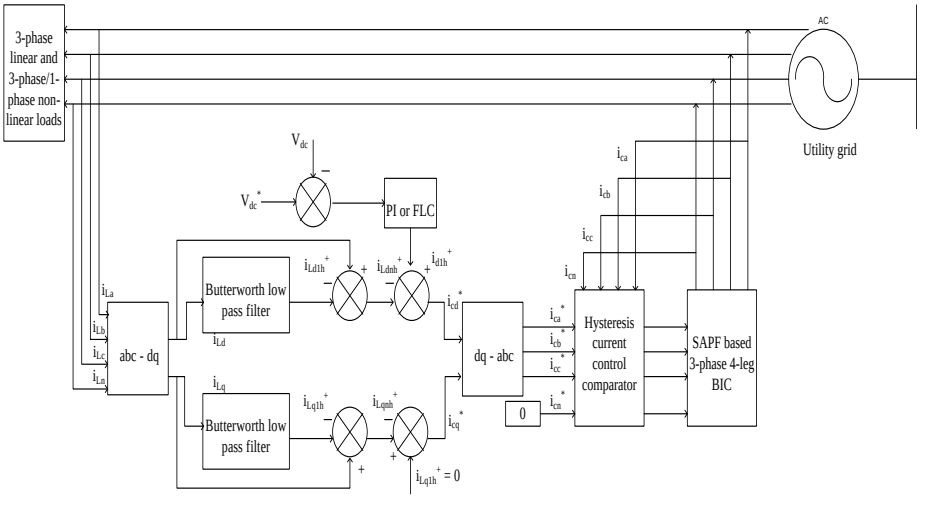

Fig. 3. d-q reference current method.

3.1. d-q Reference Current Method

The control diagram of d-q reference current method is shown in detail in Fig. 3. The determination of angle θ with respect to α – β frame is obtained by d – q frame. The transformation of d– q reference frame is illustrated as,

$$\begin{bmatrix} i_d \\ i_q \\ i_o \end{bmatrix} = \begin{bmatrix} \cos\theta & \sin\theta & 0 \\ -\sin\theta & \cos\theta & 0 \\ 0 & 0 & 1 \end{bmatrix} \begin{bmatrix} i_\alpha \\ i_\beta \\ i_o \end{bmatrix} \quad (19)$$

Each of the above currents have an average value and an oscillating value,

$$i_d = \bar{i}_d + \tilde{i}_d \quad (20)$$

$$i_q = \bar{i}_q + \tilde{i}_q \quad (21)$$

In the above equations, only the magnitude of currents is transformed and power calculations are performed on d-q-axis components. The zero sequence current components remain unchanged when the d-axis has the same direction similar to voltage space vector $\bar{v}$. Hence,

$$\begin{bmatrix} i_d \\ i_q \\ i_o \end{bmatrix} = \frac{1}{v_{\alpha\beta}} \begin{bmatrix} v_\alpha & v_\beta & 0 \\ -v_\beta & v_\alpha & 0 \\ 0 & 0 & v_{\alpha\beta} \end{bmatrix} \begin{bmatrix} i_{L\alpha} \\ i_{L\beta} \\ i_{Lo} \end{bmatrix} \quad (22)$$

The reference supply current will be determined as follows,

$$i_{sd} = \bar{i}_{Ld}; i_{sq} = i_{so} = 0 \quad (23)$$

$$i_{Ld} = \frac{v_\alpha i_{L\alpha} + v_\beta i_{L\beta}}{v_{\alpha\beta}} = \frac{P_{\alpha\beta}}{\sqrt{v_\alpha^2 + v_\beta^2}} \quad (24)$$

The average value of (24) is,

$$\bar{i}_{Ld} = \left(\frac{P_{L\alpha\beta}}{v_{\alpha\beta}}\right)_{dc} = \left(\frac{P_{L\alpha\beta}}{\sqrt{v_\alpha^2 + v_\beta^2}}\right)_{dc} \quad (25)$$

Multiplying (25) with unit vector because of reference supply current in phase with voltage at CCP,

$$i_{sref} = \bar{i}_{Ld} \frac{1}{v_{\alpha\beta}} \begin{bmatrix} v_\alpha \\ v_\beta \\ 0 \end{bmatrix} \quad (26)$$

$$\begin{bmatrix} i_{s\alpha ref} \\ i_{s\beta ref} \\ i_{sref} \end{bmatrix} = \left(\frac{P_{L\alpha\beta}}{v_{\alpha\beta}}\right)_{dc} \frac{1}{v_{\alpha\beta}} \begin{bmatrix} v_\alpha \\ v_\beta \\ v_o \end{bmatrix} \quad (27)$$

$$\begin{bmatrix} i_{s\alpha ref} \\ i_{s\beta ref} \\ i_{sref} \end{bmatrix} = \left(\frac{P_{L\alpha\beta}}{\sqrt{v_\alpha^2 + v_\beta^2}}\right)_{dc} \frac{1}{\sqrt{v_\alpha^2 + v_\beta^2}} \begin{bmatrix} v_\alpha \\ v_\beta \\ v_o \end{bmatrix} \quad (28)$$

The key benefits of $i_d - i_q$ scheme is that the angle θ is determined directly from a grid voltage source without using a PLL to synchronize. The PI control or FLC applies to the d-axis in d – q reference frame to control the small real component current and then the current controller controls this current to regulate the voltage constant across capacitor C_{dc}.

3.2. Hysteresis Current Control Comparator

The transfer of real power between AC-DC buses with the utility grid depends on the DC link voltage control. Further the working of HCC without PLL as compared to HCC with PLL [31] is discussed.

The reference neutral signal obtained from d-q reference current control is set to zero to compensate the neutral current by the 4th leg of BIC i.e,

$$i_{cn}^* = 0 \quad (29)$$

The reference signals i_{ca}^*, i_{cb}^*, i_{cc}^* and i_{cn}^* obtained from d-q reference current control are compared with actual grid currents i_{ca}, i_{cb}, i_{cc} and i_{cn} are shown below to obtain the current errors being given to the HCC to generate the switching pulses (P_1 to P_8) for BIC.

$$\begin{aligned} i_{caerr} &= i_{ca}^* - i_{ca} \\ i_{cberr} &= i_{cb}^* - i_{cb} \\ i_{ccerr} &= i_{cc}^* - i_{cc} \\ i_{cnerr} &= i_{cn}^* - i_{cn} \end{aligned} \quad (30)$$

If the current errors are above the upper bandwidth, then the upper switch of the corresponding phase leg is turned OFF, otherwise the lower switch is turned ON and vice-versa. This HCC without PLL has a very rapid response and good accuracy due to the sudden change of load and its control diagram is depicted in Fig. 4.

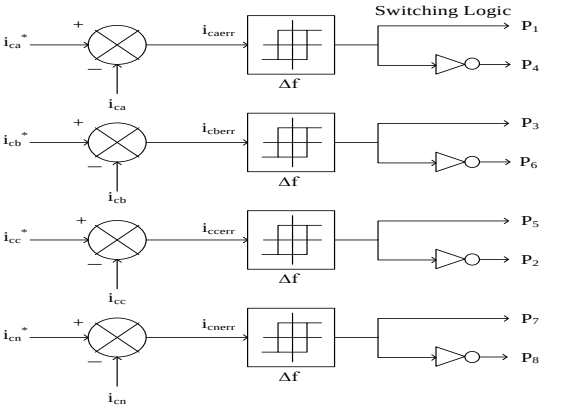

Fig. 4. Control diagram of HCC.

Table 3. Parameters used for simulation.

Parameters	Values
BIC power rating	P_{conv}=10kVA
Capacitor across the PV array	C_{pv}=110μF
Inductor for the boost converter	L_1=7.45mH
Capacitor across DC link	C_{dc}=3000μF
Switching frequency for the boost converter	f_s=20kHz
Frequency of the AC grid	f=50Hz
Voltage across the capacitor	V_{dc}=800V
Source inductance	L_s=0.01mH
Filtering inductor for the BIC	L_2=5mH
Filtering capacitor for the BIC	C_2=0.5mF
Equivalent resistance of the BIC	C_2=0.5mF

4. CASE STUDY: RESULTS AND DISCUSSION

Simulation studies have carried out using MATLAB/SIMULINK software in order to validate the coordination control of converters for the proposed AC-DC hybrid PV array and DFIG wind with the mains grid to supply continuous, highly efficient and quality power to the variable DC load and variable AC linear and non-linear loads. The PV array is simulated at various solar irradiation whereas DFIG wind at various wind speed and the other parameters for the AC-DC HM is tabulated in Table 3.

4.1. Performance of d-q Reference Current Method under Balanced Grid, Linear and Non-linear Load Condition

Case 4.1(i): BIC is in rest mode

In this case, initially the unfiltered grid current and the DFIG current is equal to the load current, as shown in Fig. 5(d). The proposed d-q reference current control produces filtered current and is

injected to the network through the BIC while regulating the dc link voltage using PI control, as shown in Fig. 5(c). This technique plays the main role in exchanging the real power between AC-DC sub-grids. Furthermore, the filtered current results in limiting the harmonics to become sinusoidal balanced grid current from the polluted grid current, as shown in Fig. 5(b). The corresponding grid voltage is shown in Fig. 5(a).

The DC load demand, P_{dcload} is fulfilled by PV, P_{pv} at 400 W/m^2 shown in Fig. 5(e). A balanced AC linear, $P_{linearload}$ and non-linear load, $P_{non\text{-}linearload}$ demands are met by DFIG wind, P_{wind} at 9 m/s, and the grid, P_{grid} supplies/receives zero power as shown in Fig. 5(f). At this instant, the BIC is in rest mode, hence P_{conv} also shown in Fig. 5(e). The grid current THD before and after filtering is shown in Fig. 5(g) and 5(h).

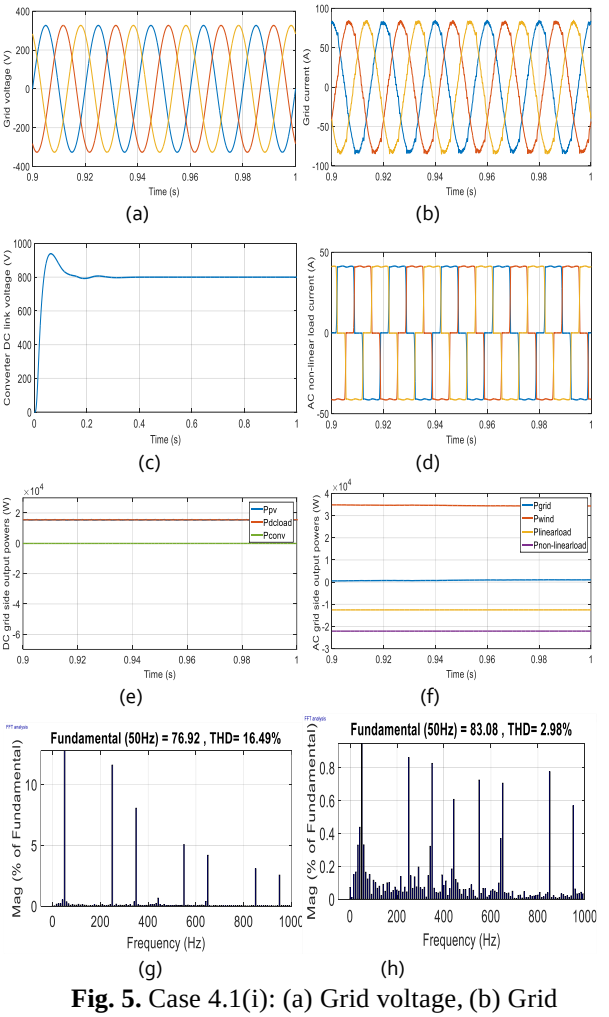

Fig. 5. Case 4.1(i): (a) Grid voltage, (b) Grid current, (c) Grid and load neutral current, (d) Converter DC link voltage, (e) AC and DC grid side output powers, (f) Non-linear load current, (g) Grid current THD before filtering and (h) Grid current THD after filtering.

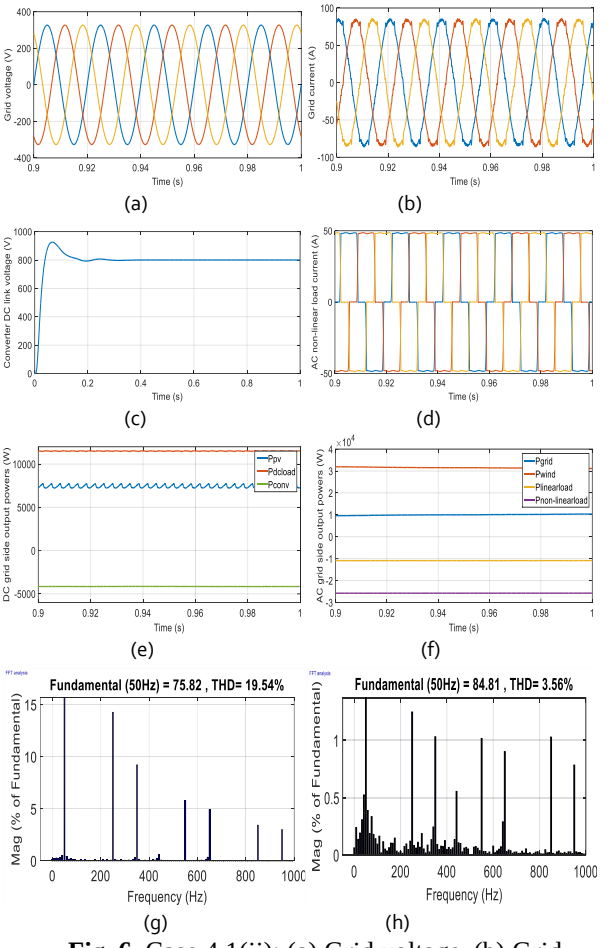

Fig. 6. Case 4.1(ii): (a) Grid voltage, (b) Grid current, (c) Grid and load neutral current, (d) Converter DC link voltage, (e) AC and DC grid side output powers, (f) Non-linear load current, (g) Grid current THD before filtering and (h) Grid current THD after filtering.

Case 4.1(ii): BIC operates in rectifier mode

In this case, initially without filtering the grid current and DFIG current is equal to the load current shown in Fig. 6(d). With filtering, the filter current starts injection to the network through the BIC and the PI control regulates the dc link voltage shown in Fig. 6(c). This results in proper real power exchange between AC-DC sub-grids. Further, the balanced grid current becomes sinusoidal from the distortion due to the presence of lower order harmonics as shown in Fig. 6(b) and the corresponding grid voltage is shown in Fig. 6(a).

The DC load demand, P_{dcload} is more than the PV power output, P_{pv} at 200 W/m^2 is shown in Fig. 6(e). A balanced AC linear, $P_{linearload}$ and non-linear load, $P_{non\text{-}linearload}$ demands are more than the DFIG wind output power, P_{wind} at 7 m/s, then the grid, P_{grid} is

supplying remaining power to both DC load and AC load, as shown in Fig. 6(f). At this instant, the BIC acts as a rectifier mode starts to supply required power, P_{conv} from the grid is shown in Fig. 6(e). The grid current THD before and after filtering is shown in Fig. 6(g) and 6(h).

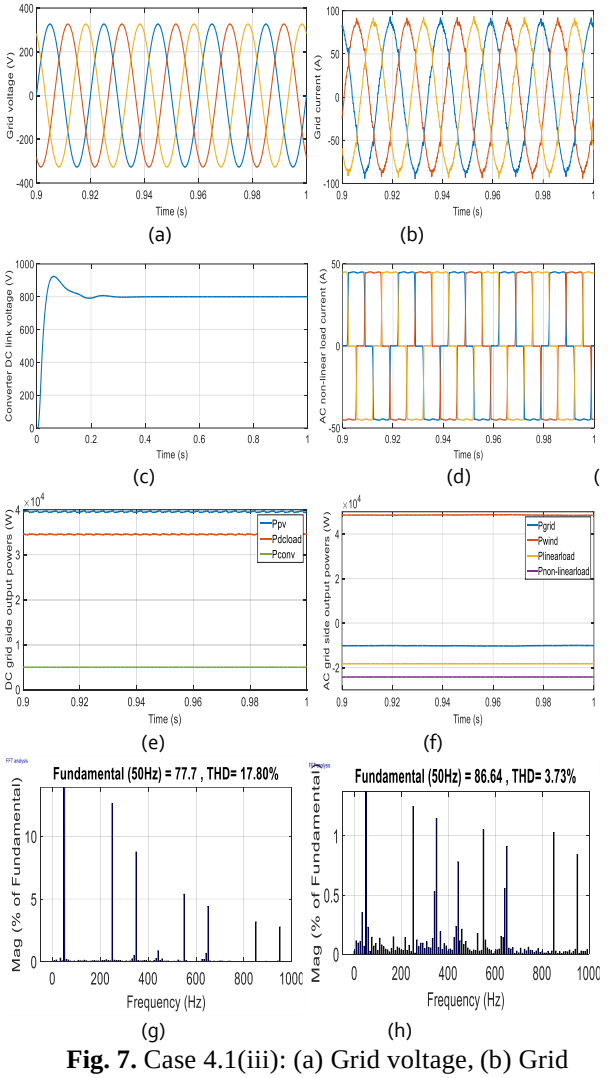

Fig. 7. Case 4.1(iii): (a) Grid voltage, (b) Grid current, (c) Grid and load neutral current, (d) Converter DC link voltage, (e) AC and DC grid side output powers, (f) Non-linear load current, (g) Grid current THD before filtering and (h) Grid current THD after filtering.

Case 4.1(iii): BIC operates in inverter mode

In this case, initially before filtering, the distorted grid current and DFIG current are equal to the load current, as shown in Fig. 7(d). After filtering, the filter current starts injection to the network through the BIC. The PI control regulates the dc link voltage shown in Fig. 7(c) which plays a main role in exchanging the optimal power between AC-DC subgrids. Further, the sinusoidal balanced grid current is obtained due to the filtered current injected to the network is shown in Fig. 7(b) and the corresponding grid voltage is shown in Fig. 7(a).

The DC load demand, P_{dcload} is less than the PV power output, P_{pv} at 1000 W/m^2 is shown in Fig. 7(e). A balanced AC linear, $P_{linearload}$ and non-linear load, $P_{non\text{-}linearload}$ demands are less than the DFIG wind output power, P_{wind} at 7 m/s, then the grid, P_{grid} is receiving surplus power from the both PV and DFIG wind shown in Fig. 7(f). At this instant, the BIC acts as an inverter mode and starts to supply extra power, P_{conv} to the grid, as shown in Fig. 7(e). The grid current THD before and after filtering is shown in Fig. 7(g) and 7(h).

4.2. Performance of d-q Reference Current Method under Unbalanced Grid, Linear and Non-linear Load Condition

Case 4.2(i): BIC is in rest mode

In this case, initially before applying the proposed d-q reference current controller to the BIC, the distorted grid current and DFIG current is equal to the load current as shown in Fig. 8(d). After applying the proposed controller to the BIC, the filter current starts injection to the network through the BIC. The PI control regulates the dc link voltage shown in Fig. 8(c) which plays a main role in exchanging the optimal power between AC-DC subgrids. Further, the sinusoidal unbalanced grid current is obtained due to the filtered current injected to the network, as shown in Fig. 8(b) and the corresponding grid voltage is shown in Fig. 8(a).

The DC load demand, P_{dcload} is satisfied by only PV, P_{pv} at 400 W/m^2 shown in Fig. 8(e). The unbalanced AC linear, $P_{linearload}$ and non-linear load, $P_{non\text{-}linearload}$ demands are satisfied by only DFIG wind, P_{wind} at 9 m/s, and hence the grid, P_{grid} supplies/receives zero power as shown in Fig. 8(f). At this instant, the BIC is in rest mode, hence P_{conv} also shown in Fig. 8(e). The grid current THD before and after filtering is shown in Fig. 8(g) and 8(h).

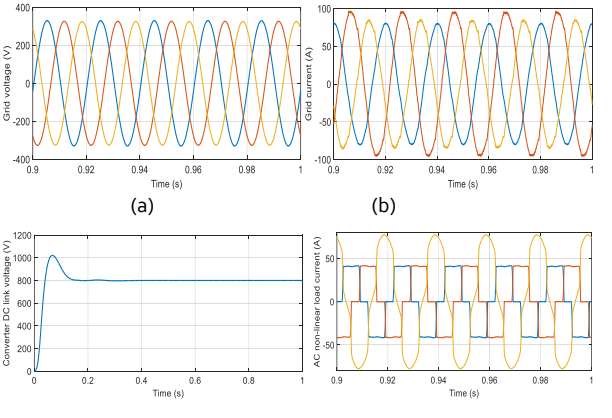

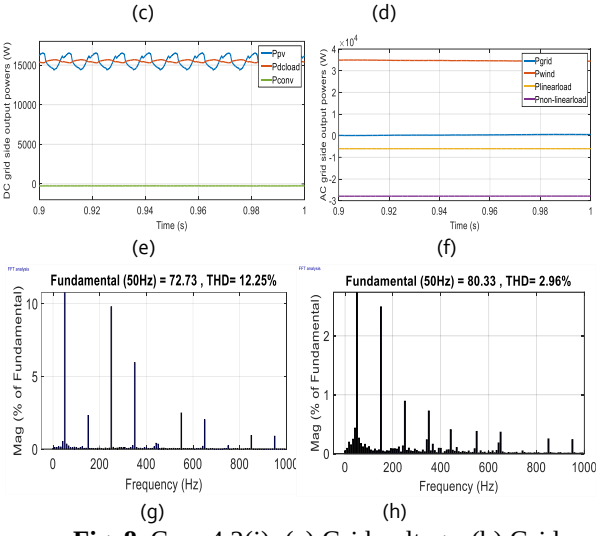

Fig. 8. Case 4.2(i): (a) Grid voltage, (b) Grid current, (c) Grid and load neutral current, (d) Converter DC link voltage, (e) AC and DC grid side output powers, (f) Non-linear load current, (g) Grid current THD before filtering and (h) Grid current THD after filtering.

Case 4.2(ii): BIC operates in rectifier mode

In this case, initially without filtering the grid current and DFIG current are equal to the load current shown in Fig. 9(d). With filtering, the filter current starts injection to the network through the BIC and the PI control regulates the dc link voltage shown in Fig. 9(c). This results in proper real power exchange between AC-DC sub-grids. Further, the unbalanced grid current becomes sinusoidal from the distortion due to the presence of lower order harmonics as shown in Fig. 9(b) and the corresponding grid voltage is shown in Fig. 9(a). The DC load demand, P_{dcload} is more than the generation of PV, P_{pv} at 200 W/m^2 shown in Fig. 9(e). The unbalanced AC linear, $P_{linearload}$ and non-linear load, $P_{non\text{-}linearload}$ demands are more than the generation of DFIG wind, P_{wind} at 7 m/s, then the grid, P_{grid} is supplying remaining power to the both DC load and AC load shown in Fig. 9(f). At this instant, the BIC acts as a rectifier mode starts to supply required power, P_{conv} from the grid also shown in Fig. 9(e). The grid current THD before and after filtering is shown in Fig. 9(g) and 9(h).

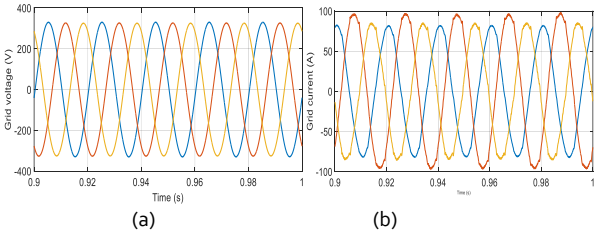

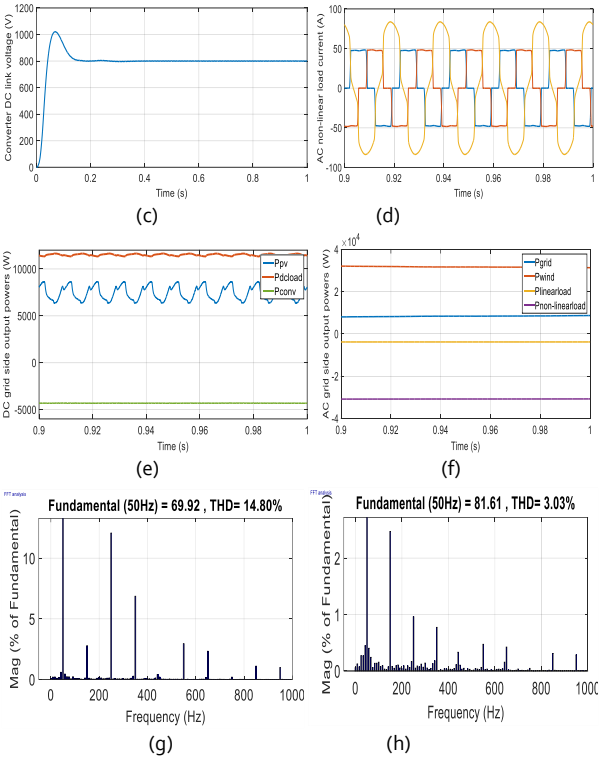

Fig. 9. Case 4.2(ii): (a) Grid voltage, (b) Grid current, (c) Grid and load neutral current, (d) Converter DC link voltage, (e) AC and DC grid side output powers, (f) Non-linear load current, (g) Grid current THD before filtering and (h) Grid current THD after filtering.

Case 4.2(iii): BIC operates in inverter mode

In this case, initially the unfiltered grid current and the DFIG current are equal to the load current, as shown in Fig. 10(d). The proposed d-q reference current control produces filtered current and is injected to the network through the BIC and also regulate the dc link voltage using PI control as shown in Fig. 10(c). These play the main role in exchanging the real power between AC-DC sub-grids. Further, the filtered current results in limiting the harmonics to become sinusoidal unbalanced grid current from the polluted grid current as shown in Fig. 10(b) and the corresponding grid voltage is shown in Fig. 10(a).

The DC load demand, P_{dcload} is less than the generation of PV, P_{pv} at 1000 W/m^2 shown in Fig. 10(e). An AC linear, $P_{linearload}$ and non-linear load, $P_{non\text{-}linearload}$ demands are less than the generation of DFIG wind, P_{wind} at 7 m/s, then the grid, P_{grid} is receiving surplus power from the both PV and DFIG wind shown in Fig. 10(f). At this instant, the BIC is acting as an inverter mode and starts to supply extra power, P_{conv} to the grid also shown in Fig. 10(e). The grid current THD before and after filtering is shown in Fig. 10(g) and 10(h).

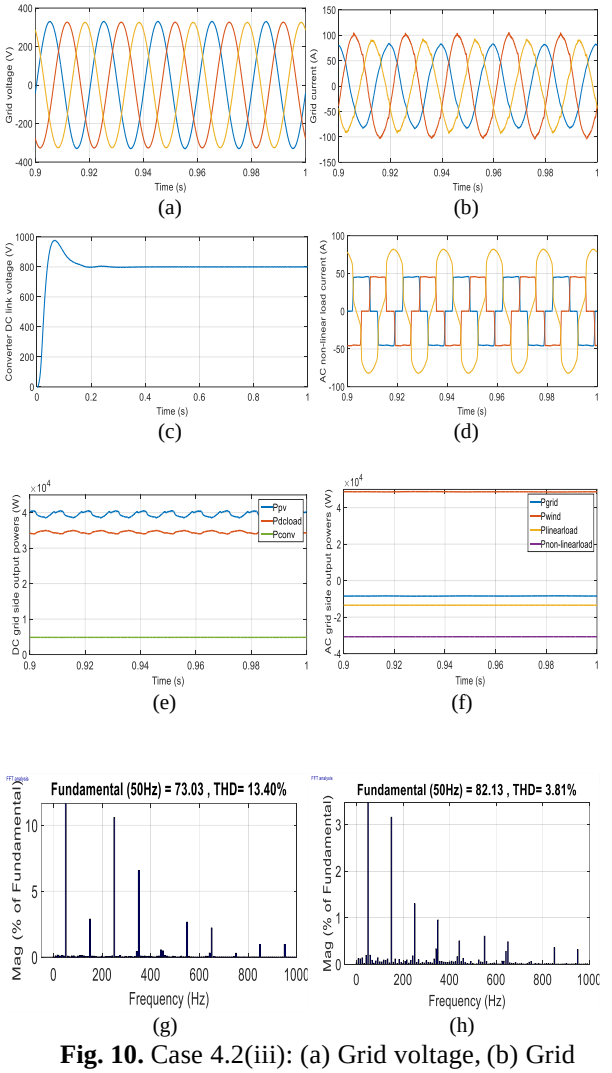

Fig. 10. Case 4.2(iii): (a) Grid voltage, (b) Grid current, (c) Grid and load neutral current, (d) Converter DC link voltage, (e) AC and DC grid side output powers, (f) Non-linear load current, (g) Grid current THD before filtering and (h) Grid current THD after filtering.

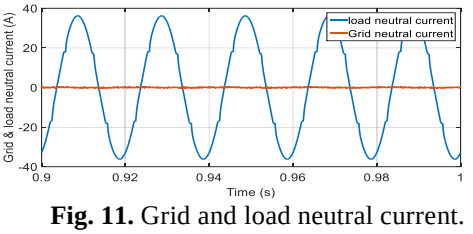

Fig. 11. Grid and load neutral current.

In the case of unbalanced load (linear and non-linear) on the AC grid side, the filter current flows to the CCP through the 4th leg of BIC to compensate the neutral current as depicted in Fig. 11. In both case 4.1 and 4.2, the results prove that the proposed controller performs efficiently with minimum power conversions in order to improve the power quality. The d-q reference current method validates its performance to maintain the grid current THD within the limits as per IEEE standards which have been summarized in Table 4.

Table 4. Performance of d-q reference current method.

Grid and load conditions	Cases	Grid current THD (%)	
		Before filtering	After filtering
Balanced	Case 4.1(i)	16.49	2.98
	Case 4.1(ii)	19.54	3.56
	Case 4.1(iii)	17.80	3.73
Unbalanced	Case 4.2(i)	12.25	2.96
	Case 4.2(ii)	14.80	3.03
	Case 4.2(iii)	13.40	3.81

5. CONCLUSIONS

In this paper, an AC-DC HM structure and the corresponding control methods for the efficient coordination of converters are studied and simulated in MATLAB/SIMULINK. The proposed structure achieves simultaneous inverter-based and rectifier-based power exchange between AC and DC sub-grids with harmonic current compensation and neutral current compensation under various grid and load conditions. In both case A and case B, as discussed in section 4, the obtained results are satisfactory and have shown that the bidirectional power flow applications with grid current harmonics at CCP within the limits as per IEEE standard. Besides, the overall AC-DC HM system is improved with minimum DC-AC-DC/AC-DC-AC conversion losses. Based on the present dominated AC power system, this AC-DC HM structure experience more practical problems to implement with utility grid but having good scope in the near future to fulfil the customers demand due to over load demand especially in India and China. The future scope of this paper will be focusing on the control strategies for isolated AC-DC HM under various grid and load conditions to provide the highly efficient and quality power at the end users in the smart distribution system.

REFERENCES

[1] O. Prakash and A.G. Shaik, **"Topological Aspects of Power Quality Improvement Techniques : A Comprehensive Overview,"** *Renew. Sustain. Energy Rev.*, Vol. 58, pp. 1129–1142, 2016.

[2] P. García-triviño, A.J. Gil-mena, F. Llorens-iborra, C.A. García-vázquez, L.M. Fernández-ramírez, and F. Jurado, **"Power Control Based on Particle Swarm Optimization of Grid-Connected Inverter for**

Hybrid Renewable Energy System," *Energy Convers. Manag.*, Vol. 91, pp. 83–92, 2015.

[3] V. Rajasekaran, A. Merabet, H. Ibrahim, R. Beguenane, and J.S. Thongam, **"Control System for Hybrid Wind Diesel Based Microgrid,"** *in Proc. 2013 IEEE Electrical Power and Energy Conf.*, pp. 1–6.

[4] W. Al-saedi, S.W. Lachowicz, D. Habibi, and O. Bass, **"Power Flow Control in Grid-Connected Microgrid Operation using Particle Swarm Optimization under Variable Load Conditions,"** *Electrical Power and Energy Systems*, Vol. 49, pp. 76–85, 2013.

[5] S. Dasgupta, S. Member, S.N. Mohan, and S. Member, **"Application of Four-Switch-Based Three-Phase Grid-Connected Inverter to Connect Renewable Energy Source to a Generalized Unbalanced Microgrid System,"** *IEEE Trans. Ind. Electron.*, Vol. 60, No. 3, pp. 1204–1215, 2013.

A. Karabiber, C. Keles, A. Kaygusuz, and B.B. Alagoz, **"An Approach for the Integration of Renewable Distributed Generation in Hybrid DC/AC Microgrids,"** *Renew. Energy*, Vol. 52, pp. 251–259, 2013.

[6] Khorsandi, M. Ashourloo, and H. Mokhtari, **"A Decentralized Control Method for a Low-Voltage,"** *IEEE Trans. Energy Convers.*, Vol. 29, No. 4, pp. 793–801, 2014.

[7] M. Kumar, S.C. Srivastava, and S.N. Singh, **"Control Strategies of a DC Microgrid for Grid Connected and Island Operations,"** *IEEE Trans. Smart Grid*, Vol. 70, No. 4, pp. 635–655, 2015.

[8] K. Strunz, E. Abbasi, and D.N. Huu, **"DC Microgrid for Wind and Solar Power Integration,"** *IEEE Journal of Emer. and Selected Topics in Power Electron.*, Vol. 2, No. 1, pp. 115–126, 2014.

[9] S. Anand, B.G. Fernandes, and J.M. Guerrero, **"Distributed Control to Ensure Proportional Load Sharing and Improve Voltage Regulation in Low-Voltage DC Microgrids,"** *IEEE Trans. Power Electron.*, Vol. 28, No. 4, pp. 1900–1913, 2013.

[10] N. Eghtedarpour and E. Farjah, **"Power Control and Management in a Hybrid AC/DC Microgrid,"** *IEEE Trans. Smart Grid*, Vol. 5, No. 3, pp. 1494–1505, 2014.

[11] X. Liu, P. Wang, and P.C. Loh, **"A Hybrid AC/DC Micro-Grid and Its Coordination Control,"** *IEEE Trans. Smart Grid*, Vol. 2, No. 2, pp. 746–751, 2011.

[12] P. Wang, L. Goel, X. Liu, F.H. Choo, and B.P. Wang, **"Harmonizing AC and DC,"** *IEEE Power and Energy Mag*, pp. 76–83, 2013.

[13] S. Pati, K. B. Mohanty, S. Kar, and A. Choudhury, **"Integration and Power Control of a Micro-Hydro-PV- Wind based Hybrid Microgrid,"** *in Proc. 2017 Int. Conf. on Circuit, Power and Computing Technologies*, pp. 1–6.

[14] F. Nejabatkhah and Y.W. Li, **"Overview of Power Management Strategies of Hybrid AC and DC Microgrid,"** *IEEE Trans. Power Electron.*, Vol. 30, No. 12, pp. 7072–7089, 2015.

[15] E. Unamuno and J.A. Barrena, **"Hybrid ac/dc microgrids — Part I : Review and classification of topologies,"** *Renew. Sustain. Energy Rev.*, Vol. 52, pp. 1251–1259, 2015.

[16] E. Unamuno and J.A. Barrena, **"Hybrid ac/dc Microgrids — Part II : Review and Classification of Control Strategies,"** *Renew. Sustain. Energy Rev.*, Vol. 52, pp. 1123–1134, 2015.

A. Gaillard, P. Poure, S. Saadate, and M. Machmoum, **"Variable speed DFIG wind Energy System for Power Generation and Harmonic Current Mitigation,"** *Renew. Energy*, Vol. 34, pp. 1545–1553, 2009.

[17] J. Hu, J. Zhu, and D.G. Dorrell, **"Predictive Direct Power Control of Doubly Fed Induction Generators Under Unbalanced Grid Voltage Conditions for Power Quality Improvement,"** *IEEE Trans. Sustain. Energy*, Vol. 6, No. 3, pp. 943–950, 2015.

[18] M. Boutoubat, L. Mokrani, and M. Machmoum, **"Control of a Wind Energy Conversion System Equipped by a DFIG for Active Power Generation and Power Quality Improvement,"** *Renew. Energy*, Vol. 50, pp. 378–386, 2013.

[19] C.-T. Hsu, R. Korimara, and T.-J. Cheng, **"Power Quality Analysis for the Distribution Systems with a Wind Power Generation System,"** *Comput. Electr. Eng*, Vol. 54, pp. 131–136, 2015.

[20] M. Singh, V. Khadkikar, A. Chandra, and R. K. Varma, **"Grid Interconnection of Renewable Energy Sources at the Distribution Level with Power-Quality Improvement Features,"** *IEEE Trans Power Electron*, Vol. 26, No. 1, pp. 307–315, 2011.

[21] M. Mehrasa, E. Pouresmaeil, S. Zabihi, E. M. G. Rodrigues, and J. P. S. Catalão, **"A Control Strategy for the Stable Operation of Shunt Active Power Filters in Power Grids,"** *Energy*, Vol. 96, pp. 325–334, 2016.

[22] Q. N. Trinh and H. H. Lee, **"An Enhanced Grid Current Compensator for Grid-Connected Distributed Generation Under Nonlinear Loads and Grid Voltage Distortions,"** *IEEE Trans. Ind. Electron.*, vol. 61, No. 12, pp. 6528–6537, 2014.

[23] E. Pouresmaeil, M. F. Akorede, D. Montesinos-Miracle, O. Gomis-Bellmunt, and J. C. Trujillo Caballero, **"Hysteresis Current Control Technique of VSI for Compensation of Grid-Connected Unbalanced Loads,"** *Electr. Eng.*, Vol. 96, No. 1, pp. 27–35, 2014.

[24] J. He, Y. W. Li, F. Blaabjerg, and X. Wang, **"Active Harmonic Filtering using Current-Controlled, Grid-Connected DG Units With Closed-Loop Power Control,"** *IEEE Trans. Power Electron.*, Vol. 29, No. 2, pp. 642–653, 2014.

[25] M. Mehrasa, E. Pouresmaeil, M. Funsho, and B. Nørregaard, **"Multilevel Converter Control Approach of Active Power Filter for Harmonics Elimination in Electric Grids,"** *Energy*, Vol. 84, pp. 722–731, 2015.

[26] G. Mehta and S.P. Singh, **"Power Quality Improvement Through Grid Integration of Renewable Energy Sources Power Quality Improvement Through Grid Integration of Renewable Energy Sources,"** *IETE Journal of Research*, Vol. 59, No. 3, pp. 210–218, 2013.

[27] M. G. Villalva, J. R. Gazoli, and E. R. Filho, **"Comprehensive Approach to Modeling and Simulation of Photovoltaic Arrays,"** *IEEE Trans. Power Electron.*, Vol. 24, No. 5, pp. 1198–1208, 2009.

[28] F.F. Rakotomananandro, **"Study of Photovoltaic System,"** Master dissertation, The Ohio State University, Ohio, 2011.

[29] Ö. C. Özerdem, S. K. Khadem, S. Biricik, M. Basu, and S. Redif, **"Real-time Control of Shunt Active Power Filter under Distorted Grid Voltage And Unbalanced Load Condition using Self-Tuning Filter,"** *IET Power Electron.*, Vol. 7, No. 7, pp. 1895–1905, 2014.